CHARACTERISATION OF BONE-REGENERATING SCAFFOLDS PRODUCED THROUGH LITHOGRAPHY-BASED CERAMIC MANUFACTURING

M. Moletsane[1*], W. du Preez[2], D. de Beer[2] & S. Nkhwa[3]

ARTICLE INFO

Article details
Presented at the 24th Annual International Conference of the Rapid Product Development Association of South Africa (RAPDASA) Institute for Industrial Engineering, held from 30 October to 2 November 2023 in Pretoria, South Africa

Available online 14 Dec 2023

Contact details
* Corresponding author
mmoletsane@cut.ac.za

Author affiliations
1 Department of Mechanical and Mechatronics Engineering, Faculty of Engineering, Central University of Technology, Bloemfontein, South Africa

2 Centre for Rapid Prototyping and Manufacturing, Faculty of Engineering, Central University of Technology, Bloemfontein, South Africa

3 Department of Biomedical Sciences, Faculty of Medicine, University of Botswana, Gaborone, Botswana

ORCID® identifiers
M. Moletsane
https://orcid.org/0000-0001-7775-4474

W. du Preez
https://orcid.org/0000-0001-9935-7330

D. de Beer
https://orcid.org/0000-0003-0175-9556

S. Nkhwa
https://orcid.org/0000-0003-0582-225X

DOI
http://dx.doi.org//10.7166/34-4-2984

ABSTRACT

Lithography-based ceramic manufacturing (LCM) is an additive manufacturing (AM) technology that builds custom-designed, three-dimensional ceramic parts layer by layer. The level of precision of the process allows for the printing of custom-made interconnected lattices and designs suitable for bone implants. This study investigated the LCM printability of various lattice structures with the hydroxyapatite (HA480) supplied by Lithoz. Different lattice structures were characterised. The microscopic structure, the composition, and the surface roughness of the test specimens were determined. To obtain the mechanical properties of the structures, compression tests were performed. The observed micropores of ±3 µm and the macropores of ±320 µm were suitable for bone cell growth. The measured microhardness of HA480 was 556±25 HV in the built direction and 559±27 HV perpendicular to the built direction. The compressive strength of the rhombic dodecahedron lattice structure was 4±0.5 MPa, and was superior to other tested lattices. From the results it was concluded that lattice structures produced through LCM have the potential to be used to produce customised bone-regenerating scaffolds.

OPSOMMING

Litografie-gebaseerde keramiekvervaardiging (LCM) is 'n laagvervaardigingstegnologie (LV) wat pasgemaakte, driedimensionele keramiekonderdele laag vir laag bou. Die vlak van akkuraatheid van die proses maak voorsiening vir die druk van pasgemaakte intern-aaneenlopende roosterstrukture en ontwerpe wat geskik is vir beenimplantate. Hierdie studie het die LCM-veraardigbaarheid van verskeie roosterstrukture ondersoek met die hidroksieapatiet (HA480) verskaf deur Lithoz. Verskillende roosterstrukture is gekarakteriseer. Die mikroskopiese struktuur, die samestelling en die oppervlakrofheid van die toetsmonsters is bepaal. Om die meganiese eienskappe van die strukture te verkry, is druktoetse uitgevoer. Die waargenome mikroporieë van ±3 µm en die makroporieë van ±320 µm was geskik vir beenselgroei. Die gemete mikrohardheid van HA480 was 556±25 HV in die bourigting en 559±27 HV loodreg op die bourigting. Die druksterkte van die rombiese dodekaëderroosterstruktuur was 4±0.5 MPa, en was beter as ander getoetste roosters. Uit die resultate is tot die gevolgtrekking gekom dat roosterstrukture wat deur LCM vervaardig word, die potensiaal het om gebruik te word vir vervaardiging van pasgemaakte beenregenererende steiers.

1. INTRODUCTION

Calcium phosphates (CaPs) are biocompatible and biodegradable ceramics that are used as substitutes to repair bone abnormalities. CaPs are some of the main components found in human bone and tooth enamel. The properties of CaPs depend on their calcium and phosphorus ratio, known as the Ca/P, and ranging from 0.5 to 2. A lower ratio indicates that the material is highly soluble and is more acidic when implanted in the human body. Material with a ratio of less than 1 is not suggested for biological implantation [1,2]. On the other hand, material with a high Ca/P ratio degrades slowly, allowing bone regeneration until the bone has healed fully. The most frequently used CaPs are hydroxyapatite (HA) with a Ca/P ratio of 1.67 and tricalcium phosphate (TCP) with a Ca/P ratio of 1.5 [1]. Hydroxyapatite as a bio-ceramic has been used extensively for clinical bone repairs, because it has excellent biocompatibility and the ability to degrade, allowing bone generation [1]. It is used as a bone scaffold to replace a bone defect as a temporary structure until the bone has completely regenerated. A bone scaffold has to meet specific requirements such as mechanical strength, biocompatibility, appropriate pore sizes, and porosity that allows for bone cell infiltration and growth and a good degradability rate before it can be implanted [3]. Ideally, a bone scaffold structure should mimic the human bone structure. As a temporary structure, the scaffold must withstand the load and transfer load and match the host bone tissue regarding Young's modulus and compressive strength [4]. Young's modulus of human cancellous bone ranges from 0.1 to 4.5 GPa, while the compressive strength ranges from 1.5 to 38 MPa [5].

Material degradation is one of the requirements for a bone scaffold. The pore size of the scaffold has an impact on the level of degradation. The pore size can be classified into two categories: micropores with a size < 5 μm, and macropores with a size > 100 μm [6]. Micropores have a large surface area that allows ion exchange and bone protein absorption. For the effective vascularisation and migration of cells and fluids in the implanted bone scaffold, the pore size is recommended to be larger than the cell size of the osteoblasts [7]. The minimum recommended pore size for a bone substitute to promote bone growth is 100 μm. Other findings demonstrate that the minimum of 300 μm is still acceptable for bone growth, however, raising the minimum pore size puts the mechanical strength of the scaffold at risk [8,9]. To achieve the desired porosity of the scaffold, it is designed with a lattice structure – that is, a porous and three-dimensional structure composed of repeating interconnected cells, struts, and nodes [10]. The design of one unit cell of the lattice structure determines the geometry of the pores that the scaffold will have. For strut-based lattice structures, when the curvature between the struts is increased, the lattice becomes ideal for cell proliferation [11]. At cellular level, the lattice structure can be manipulated by changing the connectivity, cell size, or strut dimensions [12-14]. On the level of the lattice structure unit cell, the deformation and failure of lattice structures has been classified on the basis of Maxwell stability. This depends on the number of struts and nodes per unit cell. According to the Maxwell (M) criterion, the unit cell is bending- (M<0) or stretching-dominated (M>0). Bending-dominated structures can endure large deformation at a lower stress level, whereas stretch-dominated structures are for a lightweight design with expected high levels of stiffness and strength. The mechanical structure expected from a lattice structure can be predicted by using the Maxwell equation:

$$M=b-3j+6 \qquad (1)$$

where b is the number of struts and j is the number of nodes [10, 15].

In the past, complex structures have been limited to being manufactured by traditional hydroxyapatite processes such as freeze-drying, sol-gel, and gas foaming [16]. However, additive manufacturing (AM) provides the freedom to have control over the complex geometrical detail of the scaffold according to a patient's bone defect [4]. Porous ceramics have been successfully produced using digital light processing (DLP) AM technology, also known as lithography-based ceramic manufacturing (LCM) [17]. LCM provides the ability to design and build customised implants with the required geometry and internal structure. LCM is an additive manufacturing process in which the building platform is immersed in a vat filled with ceramic slurry, and cured layer by layer with UV light to build a complete three-dimensional part [17].

Recently LCM has been used to produce ceramic scaffolds such as zirconia [18], HA/ tricalcium phosphate [19], and tricalcium phosphate [20]. Hydroxyapatite bone scaffolds were successfully manufactured via DLP with a ceramic specimen density of 90% [21]. Bone-like hydroxyapatite were successfully printed using the CeraFab 7500 LCM system, with pores ranging from 100 to 800 μm [22]. An evaluation of the mechanical properties of LCM-HA-printed octahedral, circular, and frame lattice structures showed good compressive strength [23]. HA manufactured by DLP (LCM) showed potential for bone regenerating scaffolds, with the

results demonstrating osteoblast proliferation, adhesion, and differentiation [21]. In this study, pore sizes of 300 to 600 µm did not compromise the mechanical strength of the porous structure.

This study investigated the feasibility of building bone-regenerating scaffolds in hydroxyapatite HA480 supplied by Lithoz GmbH for additive manufacturing (AM) ceramics through the LCM technology. The HA480 material is a recent improvement from Lithoz of the HA400 ceramic. This study aimed to test this new material for application as a bone regeneration scaffold. High-precision green body lattice structures were prepared and sintered. The surface morphology of the lattice structures was analysed and the surface roughness was measured to assess its potential to promote cell adhesion. Micropores and macropores suitable for stimulating cell growth were found. The physical and mechanical properties of HA480 showed that the material could be used for bone regeneration scaffolds for cancellous bone substitution.

2. METHODOLOGY

2.1. HA480 slurry preparation

The process of creating the slurry began by using the commercially available HA ($[Ca_{10}(PO_4)_6](OH)_2$) powders repared by Lithoz GmbH. These HA powders were dried for about 24 hours at 120°C and added in three steps to the separately prepared organic matrix containing solvent, reactive monomers, and photo initiator (usually less than 1 wt%). At each step a precise amount of powder was added to the matrix to create a homogeneous slurry. The SpeedMixerTM DAC 400.1 FVZ (Hauschild, Germany) was used for this process. The slurry was mixed for 30 seconds at 1 800 rpm and then for 30 seconds at 2 750 rpm. When all of the powder had been added to the binder, the slurry underwent a dispersion process with milling beads for three hours. A rheology additive was added to the ready-for-use slurry to bring stability [24]. The HA powder size and binder name were not disclosed by the supplier.

2.2. Scaffold design and manufacturing

The LCM fabrication process was conducted with the HA480 slurry by using a CeraFab S65 machine at Lithoz, as shown in Figure 1. First, the CAD models of the test specimens were designed using Magics® software, based on the unit cells in Figure 2. The CAD models were processed using the data preparation software of the CeraFab S65 printer, where the orientation of the part on the building platform and suitable printing parameters were selected. A shrinkage compensation factor was also added in the X, Y, and Z directions before printing the samples according to the material parameters. The samples were printed using a layer thickness of 25 µm, as specified in the supplier's manual. During the printing process, the material was cured by UV light layer-by-layer, resulting in green state parts. The HA480-printed green parts were heat-treated in a Nabertherm professional muffle furnace L40/110 to remove the binder and then sinter the green parts at a temperature of 1 300 °C for two hours.

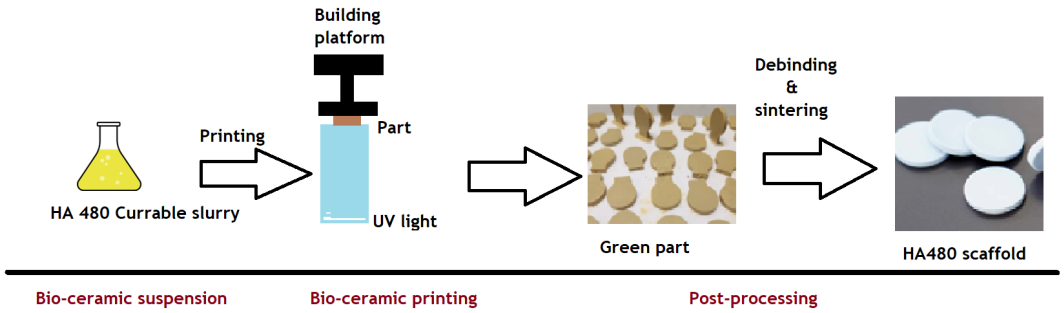

Figure 1: Systematic process employed in the LCM of HA480

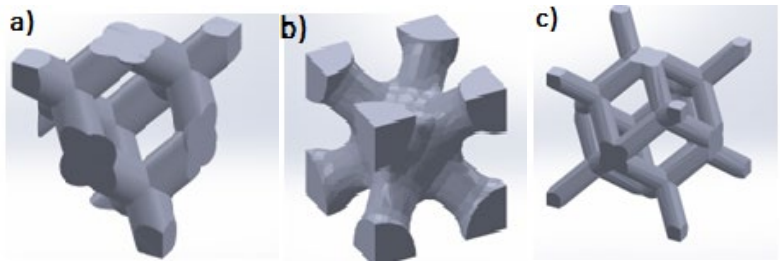

Figure 2: CAD designs for lattice unit cell structures: a) diamond, b) diagonal, and c) rhombic dodecahedron

2.3. Characterisation of samples

2.3.1. Optimising unit cell array

The strut type cell topology was classified according to the Maxwell number M. The unit cell CAD designs in Figure 2 were used for the calculation. The number of nodes and struts from each unit cell were derived and the Maxwell stability was calculated.

2.3.2. Microstructural and morphological analysis

The microstructure and pore morphology of the sintered lattice structures was analysed using a JEOL JSM-7800F scanning electron microscope (SEM). The chemical analysis and elemental mapping of the samples was conducted by using energy-dispersive X-ray spectroscopy (EDS).

Solid cell culture samples of HA480 were tested for surface roughness using a Surftest SJ 210 portable surface roughness tester. The surface roughness measurements were repeated three times on both un-sintered and sintered solid samples.

2.3.3. Shrinkage of scaffold

The shrinkage of the material was evaluated by comparing the CAD model's dimensions with those of the sintered samples. The sintered samples were measured in length, width, and thickness with a micrometer. Four samples for each lattice structure were measured, and the average was recorded. The shrinkages in the Z direction (r_{sz}) and in the XY plane (r_{sr}) were compared. Linear shrinkage was calculated by using equations 2 and 3 [25]. H is the measurement of the CAD model and Hs is the measurement of a sintered sample. The symbol D is the dimension of the CAD model and Ds is the measurement after sintering.

$$r_{sz}=\frac{H-Hs}{H} \qquad (2)$$

$$r_{sr}=\frac{D-Ds}{D} \qquad (3)$$

2.3.4. Mechanical testing

The mechanical properties of the solid HA480 were first determined by using a Vickers hardness testing machine. Forty indentations in three rows were made on the test specimens shown in Figure 3(a). Microhardness was tested both on the surface of the sample parallel to the build direction and on the surface perpendicular to the build direction. In addition, compression tests were performed on the lattice structures at a speed of 1mm/min with an MTS Criterion Model 43 universal testing machine. Three sets of dry specimens of 5 x 5 x 3 mm of the lattice structure specimens, shown in Figure 3(b), were compressed until failure.

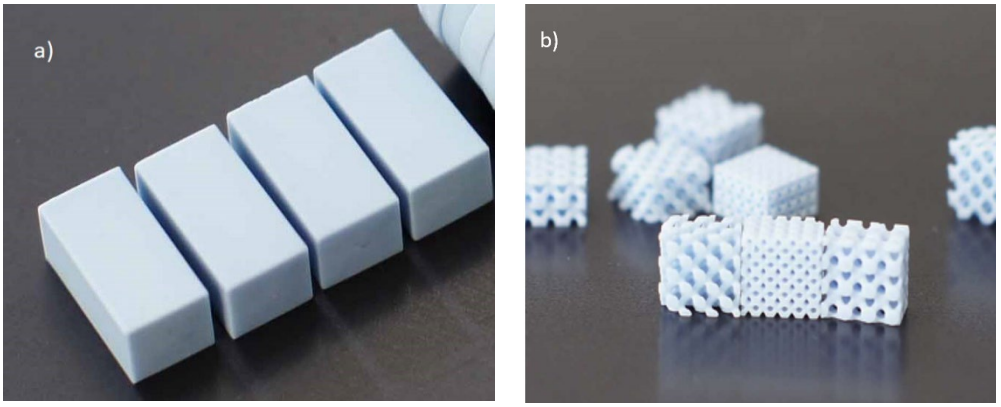

Figure 3: Mechanical test specimens: a) hardness solid specimens, b) compression lattice structure specimens

3. RESULTS AND DISCUSSION

3.1. Scaffold architecture and microstructure

3.1.1. Optimising the unit cell

The scaffold stability was optimised by calculating the Maxwell value for all three unit cells shown in Figure 2, and is given in Table 1. The results showed that the diamond lattice structure was a bending-dominated unit cell, because the Maxwell number was less than zero. Bending-dominated structures experience bending moments that can contribute to the failure of the scaffold. However, the diagonal and rhombic dodecahedron unit cells had M>0, which indicates a stretch-dominated structure. Diamond lattice structures are suitable for small to medium load-bearing scaffolds.

Table 1: Maxwell stability of unit cells

	Diamond	Diagonal	Rhombic dodecahedron
No. of nodes	7	1	12
No. of struts	9	8	48
Maxwell value	-6	11	18

3.1.2. Lattice pore size

In the SEM it was confirmed that the stacked layers of material formed a complete 3D part, as shown in Figure 4(a). All of the printed 3D lattice structures confirmed a successful additive manufacturing process. From the SEM results, micropores were evident in all the lattice structures, as illustrated in Figure 4(b). During debinding, owing to evaporated binder, micropores are formed, resulting in a large surface area that is conducive to ion exchange and bone protein. Apart from these processes, macropores are essential for vascularisation. Figure 4(c) shows the typical macropores of the diagonal lattice structure. Therefore, an LCM-produced HA bone scaffold with 300–600 μm pores would be able to promote cell growth while maintaining good mechanical strength [6].

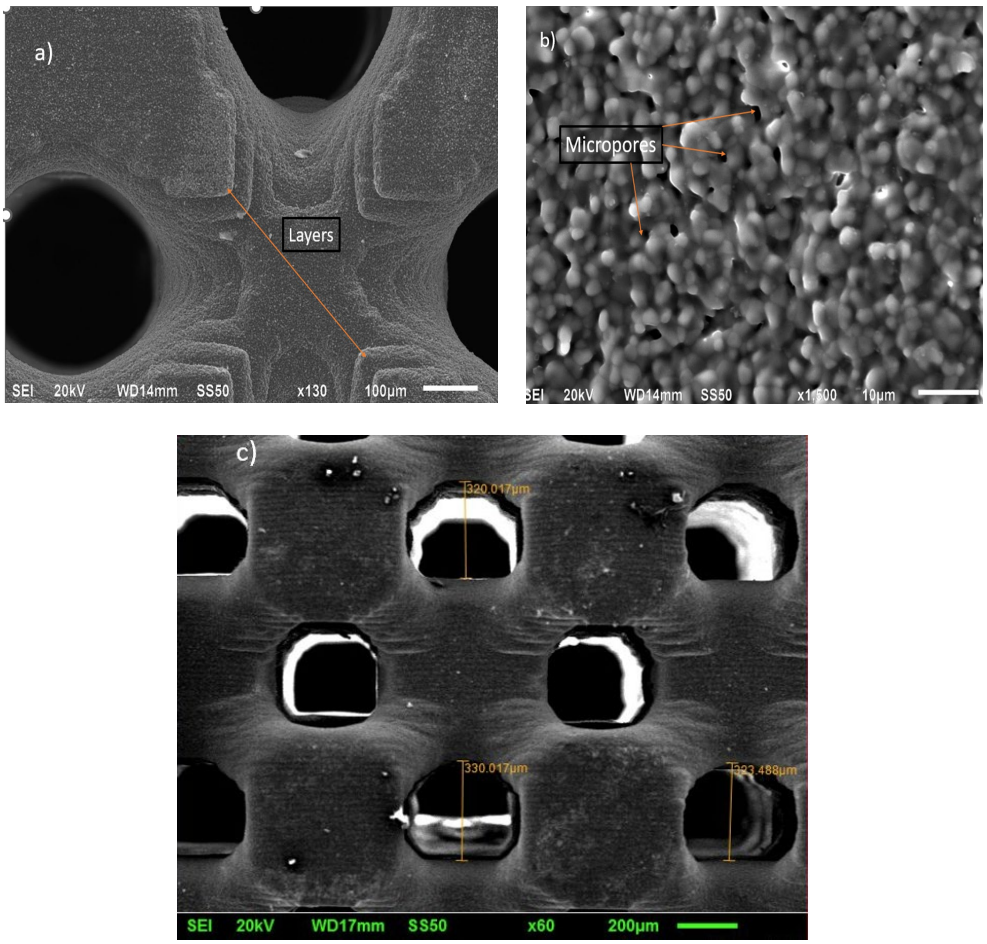

Figure 4: SEM images of a) HA480 LCM layers, b) micropores, and c) macropores of size ~300 µm for the diagonal lattice structure

3.1.3. Printing accuracy

From a comparison of the geometries of the LCM HA480 lattice structures with the CAD model's geometry, it was found that the LCM process produced accurate results. The pores in all of the lattice structures were clear of impurities and surface irregularities, as shown in Figure 5(a) and (b) for two of the structures. Therefore, the precision of this technology allows complex lattices to be printed without compromising quality; thus printing a detailed patient-specific implant for the complex geometry of a bone defect is warranted.

Normally, during the post-processing of ceramics such as hydroxyapatite, the samples experience shrinkage. During the de-binding process, the binder evaporates and the sintering process fuses the HA particles together [26,27]. In this study, a material shrinkage compensation factor was added to all of the dimensions during the design process. This allowed the fabrication of accurate pores of different sizes. The shrinkages of the samples were calculated; the results yielded a negative percentage, meaning that there was no shrinkage: instead, the samples increased in size because of the shrinkage compensation factor that was added before printing. From Table 2 it is evident that there was overcompensation for shrinkage, as indicated by the negative shrinkage values.

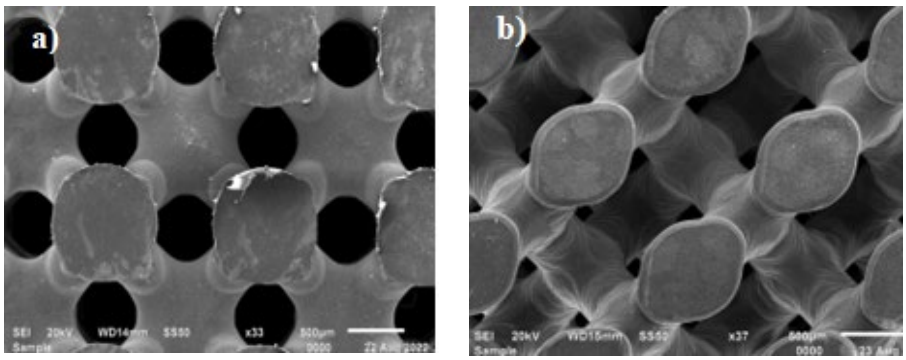

Figure 5: Printing accuracy of LCM HA480 for a) diagonal lattice and b) diamond lattice

Table 2: Calculated shrinkage percentage of the different lattice structures, based on the CAD dimensions

Diamond	Length (mm)	Width (mm)	Thickness (mm)
CAD	5	5	3
Sintered (avg.)	5.4	5.4	3.1
Shrinkage % (avg.)	-7.6	-7.8	-3.3
Standard deviation	0.2	0.2	0

Diagonal	Length (mm)	Width (mm)	Thickness (mm)
CAD	5	5	3
Sintered (avg.)	5.4	5.4	3.4
Shrinkage % (avg.)	-8.1	-7.8	-13.3
Standard deviation	0.1	0.2	0.3

Rhombic	Length (mm)	Width (mm)	Thickness (mm)
CAD	5	5	3
Sintered (avg.)	5.4	5.4	3.4
Shrinkage % (avg.)	-8.5	-8.3	-7.6
Standard deviation	0.8	0.6	0.5

In the diamond lattice structure shown in Figure 6, the first layers of the structure that were attached to the printing platform were cracked, and other sections were broken. In comparison, the top or side view layers were not affected. Removal of the samples from the building platform probably caused the breakages. Kang *et al*. [23] found that the first print layers of lattice structures had chipped edges as result of their removal from the building platform, and could initiate crack growth, resulting in premature scaffold failure. Printing supports could be recommended for such lattice structures to avoid the structure itself being damaged.

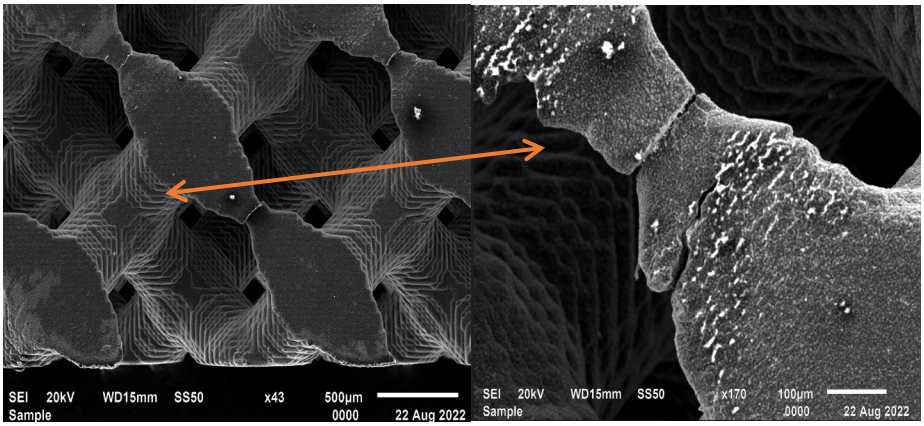

Figure 6: SEM images showing cracked first layers of the diamond lattice structure

3.1.4. Composition of the material

The composition of the LCM HA480 parts confirmed the presence of calcium phosphate that was suitable for bone regeneration. Table 3 shows the EDS of the elements that were found in additively produced HA480 at various locations on the lattice samples. The average Ca/P wt% ratio in HA480 was 1.61, which was close to the theoretical Ca/P ratio of hydroxyapatite of 1.67 [28]. Calcium phosphates are widely used for bone repair thanks to their excellent biocompatibility and their ability to bond with bone tissue at the interfaces. The typical EDS spectrum of a HA480 lattice structure shown in Figure 7 confirmed the presence of Ca, O, and P, the constituents of the biocompatible calcium phosphate phase, as they appeared in all of the lattice structures that were analysed.

Table 3: LCM HA480 elemental composition in wt% as determined through EDS

	O	P	Ca	Ca/P
Rhombic	60.6±1.35	14.1±0.16	25.1±0.25	1.79
	60.5±2.01	14.2±0.17	25.2±0.26	1.78
	60.5±0.89	18.5±0.22	24.8±0.43	1.33
	60.9±1.33	14.4 ±0.17	24.4±0.26	1.69
Diagonal	60.6±1.31	14.1±0.16	26±0.25	1.77
	60.2±0.41	18±0.20	24.4±0.41	1.35
	60.6±1.30	14±0.16	25.1±0.24	1.79
	60.6±0.4	18.9±0.22	24.6±0.43	1.33
	61±0.85	14.7±0.17	24.4±0.26	1.66
Diamond	60.1±2.50	17.9±0.50	24.8±1.00	1.39
	61.4±3.08	15.3±0.42	23.3±0.63	1.53
	60.6±3.72	14.2±0.39	25.2±0.60	1.78
	60.4±3.76	13.9±0.39	24.5±0.60	1.76
			Average	1.61

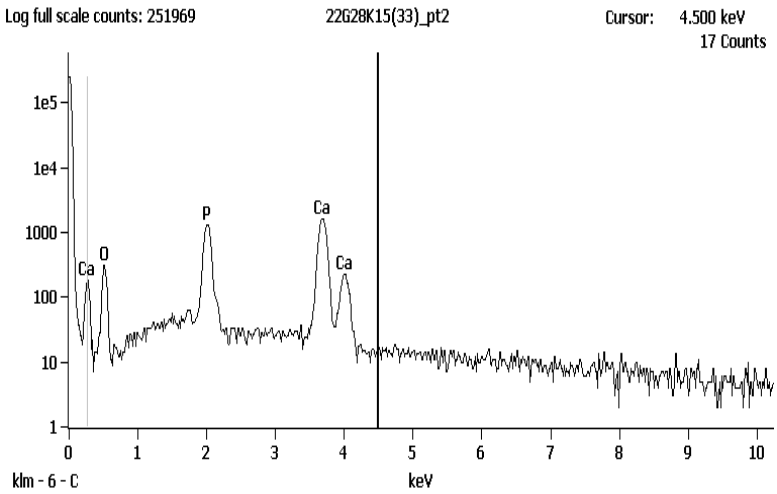

Figure 7: EDS compositional spectra of the LCM HA480

3.2. Surface roughness

The surface roughness of the LCM cell culture samples was evaluated for both the green body and the sintered states. It was found that the sintered sample had an average roughness of Ra = 0.60±0.05 µm. This Ra value was close to that of re-crushed and sintered HA (0.77 µm) [29]. The green body surface roughness was Ra = 1.20±0.38 µm. The higher Ra values for the unsintered green parts were because the unsintered samples were not yet fully dense. During debinding, the binder was evaporated, and during the sintering of the HA480 particles, final full density was achieved. The surface roughness of osteoblast cells that are appropriate for cell adhesion ranges from 0.2 to 8µm [30]. The presence of appropriate surface roughness on sintered HA480 suggests that cell adhesion and proliferation could be stimulated [31,32].

3.3. Mechanical properties

The hardness of ceramics depends on their porosity and grain size. When porosity increases, the hardness decreases [33]. The Vickers microhardness of the LCM H480 structures was found to be similar on the surfaces parallel to and perpendicular to the build direction. The average values were within the standard range of the microhardness of hydroxyapatite [2] and higher than previous AM-manufactured HA [21], shown in Table 4.

Table 4: Vickers microhardness of hydroxyapatite structures

Material	Average Vickers microhardness (HV)	Reference
HA480 on build direction surface	556±25	
HA480 on surface perpendicular to build direction	559±27	
Dense HA	300-700	[2]
AM-produced HA	160 – 280.6	[21]

The compressive strength of cancellous bone ranges from 1.5 to 38 MPa [5]. The compression results of the HA480 diagonal and rhombic dodecahedron lattice structures gave strengths higher than the minimum strength of cancellous bone. In this investigation, the rhombic dodecahedron lattice had a superior compressive strength of 4.2±0.49 MPa in comparison with the compressive strength of the diamond lattice of 0.7±0.08 MPa, as shown in Figure 8. The LCM HA480 compressive strength was within the acceptable range when compared with the porous LCM printed bone scaffolds investigated by Kang *et al*. [23]. The results from Kang *et al*. showed high strength when the HA slurry contained 35% HA powder particles by volume. The compressive strength of the LCM produced HA400 triply periodic minimal surface, and the lattice structure was found to be within the range of natural bone compressive strength but less than the results in Figure 8

[34]. The difference in the geometry of the lattice structures and the Maxwell criterion numbers compared with the literature had an influence on the compression results. The Maxwell criterion number on the unit cell influenced the lattice to bend or stretch during compression loading [15]. If the mechanical strength of the lattice needed to be improved, adjustments could be made to the unit cell.

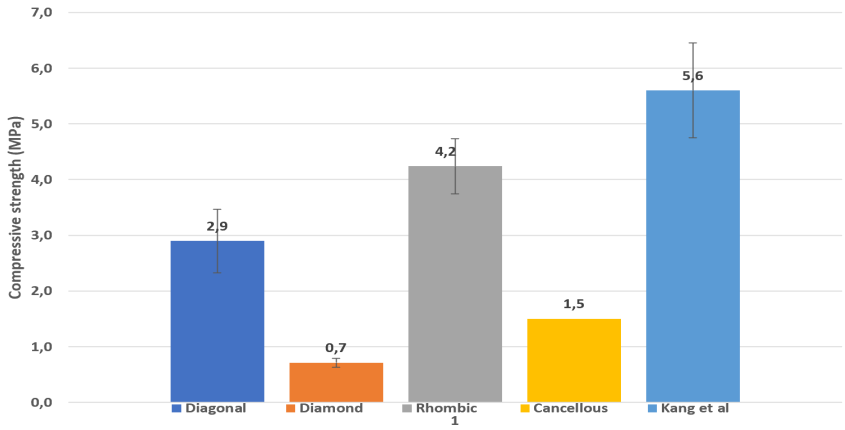

Figure 8: Compressive strength of different lattice structures

4. CONCLUSIONS

LCM lattice structures produced from HA480 powder have the potential to be used to create complex parts for bone-regeneration scaffolds. This was demonstrated by the results obtained in this study.

- The high level of precision of the LCM HA480 lattice structures produced in this study.
- The Ca/P ratio of the LCM HA480 demonstrated that the material can be used for bone regeneration, because it was almost the same as the recommended Ca/P ratio for hydroxyapatite.
- The microhardness of the LCM HA480 was 556±25 HV and 559±27 HV, both of which fall within the range of hydroxyapatite hardness values.

The rhombic dodecahedron lattice structure had a compression strength that was superior to all of the tested lattice structures and can be recommended for use as a scaffold for cancellous bone.

ACKNOWLEDGEMENTS

This work is based on research supported by the South African Research Chairs Initiative of the Department of Science and Technology and the National Research Foundation of South Africa (Grant No. 97994), the Collaborative Programme in Additive Manufacturing (Contract No. CSIR-NLC-CPAM-21-MOA-CUT-01), the Manufacturing, Engineering and Related Services Sector (merSETA) and the Central University of Technology (CUT) MoA. The funding of the Chair in Innovation and Commercialisation of Additive Manufacturing (CICAM), 21 December 2018 and the financial contribution of the New Generation of Academics Programme are gratefully acknowledged. The Centre for Rapid Prototyping and Manufacturing is also acknowledged for their technical support.

REFERENCES

[1] **E. Fiume, G. Magnaterra, A. Rahdar, E. Verné, and F. Baino**, Hydroxyapatite for biomedical applications: A short overview, *Ceramics*, 4(4), 542–563, 2021.

[2] **N. Eliaz and N. Metoki**, Calcium phosphate bioceramics: A review of their history, structure, properties, coating technologies and biomedical applications, *Materials*, 10(4), 334, 2017.

[3] **S. Kanwar and S. Vijayavenkataraman**, Design of 3D printed scaffolds for bone tissue engineering: A review, *Bioprinting*, 24, e00167, 2021.

[4] **S. Mondal and U. Pal**, 3D hydroxyapatite scaffold for bone regeneration and local drug delivery applications, *Journal of Drug Delivery Science and Technology*, 53, 101131, 2019.

[5] **C. Mangano, F. Mangano, L. Gobbi, O. Admakin, S. Iketani, and A. Giuliani**, Comparative study between laser light stereo-lithography 3D-printed and traditionally sintered biphasic calcium phosphate scaffolds by an integrated morphological, morphometric and mechanical analysis, *International Journal of Molecular Science*, 20(13), 3118, 2019.

[6] **G. Hannink and J. J. C. Arts**, Bioresorbability, porosity and mechanical strength of bone substitutes: What is optimal for bone regeneration? *Injury*, 42, S22–S25, 2011.

[7] **J. Triyono, R. Alfiansyah, H. Sukanto, D. Ariawan, and Y. Nugroho**, Fabrication and characterization of porous bone scaffold of bovine hydroxyapatite-glycerin by 3D printing technology, *Bioprinting*, 18, e00078, 2020.

[8] **Z. Liu *et al.***, Additive manufacturing of hydroxyapatite bone scaffolds via digital light processing and in vitro compatibility, *Ceramics International*, 45(8), 11079–11086, 2019.

[9] **K. Hayashi, M. L. Munar, and K. Ishikawa**, Effects of macropore size in carbonate apatite honeycomb scaffolds on bone regeneration, *Materials Science and Engineering: C*, 111, 110848, 2020.

[10] **M. Ashby**, The properties of foams and lattices, *Philosophical Transactions of the Royal Society A: Mathematical, Physical and Engineering Sciences*, 364, 15–30, 2006.

[11] **J. Knychala, N. Bouropoulos, C. Catt, O. Katsamenis, C. Please, and B. Sengers**, Pore geometry regulates early stage human bone marrow cell tissue formation and organisation, *Annals of Biomedical Engineering*, 41, 917–930, 2013.

[12] **S. Ahmadi, G. Campoli, S. Amin Yavari, B. Sajadi, R. Wauthle, J. Schrooten, H. Weinans, and A.A. Zadpoor**, Mechanical behavior of regular open-cell porous biomaterials made of diamond lattice unit cells, *Journal of the Mechanical Behavior of Biomedical Materials*, 34, 106–115, 2014.

[13] **F. Liu, D. Z. Zhang, P. Zhang, M. Zhao, and S. Jafar**, Mechanical properties of optimized diamond lattice structure for bone scaffolds fabricated via selective laser melting, *Materials*, 11(3), 374, 2018.

[14] **W. Bai, L. Shu, R. Sun, J. Xu, V. Silberschmidt, and N. Sugita**, Improvements of material removal in cortical bone via impact cutting method, *Journal of the Mechanical Behavior of Biomedical Materials*, 108, 103791, 2020.

[15] **W. Tao and M. C. Leu**, Design of lattice structure for additive manufacturing, in *2016 International Symposium on Flexible Automation (ISFA)*, pp. 325–332, 2016.

[16] **I. Adel, M. Elmeligy, and N. Elkasabgy**, Conventional and recent trends of scaffolds fabrication: A superior mode for tissue engineering, *Pharmaceutics*, 14(2), 306, 2022.

[17] **E. Schwarzer, M. Götz, D. Markova, D. Stafford, U. Scheithauer, and T. Moritz**, Lithography-based ceramic manufacturing (LCM) – Viscosity and cleaning as two quality influencing steps in the process chain of printing green parts, *Journal of the European Ceramic Society*, 37, 5329–5338, 2017.

[18] **J. Zhang, D. Huang, S. Liu, X. Dong, Y. Li, H. Zhang, Z. Yang, Q. Su, W. Huang, W. Zheng, and W. Zhou**, Zirconia toughened hydroxyapatite biocomposite formed by a DLP 3D printing process for potential bone tissue engineering, *Materials Science and Engineering: C*, 105, 110054, 2019.

[19] **H. Lim, S. Hong, S. Byeon, S. Chung, S. On, B. Yang, J. Lee, and S. Byun**, 3D-printed ceramic bone scaffolds with variable pore architectures, *International Journal of Molecular Sciences*, 21, 6942, 2020.

[20] **C. Ghayor, T. H. Chen, I. Bhattacharya, M. Özcan, and F. E. Weber**, Microporosities in 3D-printed tricalcium-phosphate-based bone substitutes enhance osteoconduction and affect osteoclastic resorption, *International Journal of Molecular Sciences*, 21(23), 9270, 2020.

[21] **Z. Liu, H. Liang, T. Shi, D. Xie, R. Chen, X. Han, L. Shen, C. Wang, and Z. Tang**, Additive manufacturing of hydroxyapatite bone scaffolds via digital light processing and in vitro compatibility, *Ceramics International*, 45(8), 11079-11086, 2019.

[22] **F. Baino, M. Giulia, F. Elisa, S. Alessandro, T. Luciana-Patricia , S. Martin, and E. Verné**, Digital light processing stereolithography of hydroxyapatite scaffolds with bone-like architecture, permeability, and mechanical properties, *Journal of the American Ceramic Society*, 105, 1648-1657, 2022.

[23] **J.-H. Kang, K. Sakthiabirami, K.- J. Jang, J.-G. Jang, G.-J. Oh, C. Park , J. G. Fisher, and S.-W. Park**, Mechanical and biological evaluation of lattice structured hydroxyapatite scaffolds produced via stereolithography additive manufacturing, *Materials & Design*, 214, 110372, 2022.

[24] **G. Magnaterra**, *Additive manufacturing of hydroxyapatite scaffolds for bone repair*, Master's thesis, Politecnico di Torino, 2020.

[25] **X. Li, Y. Yuan, L. Liu, Y.S. Leung, Y. Chen, Y. Guo, Y. Chai, and Y. Chen**, 3D printing of hydroxyapatite/tricalcium phosphate scaffold with hierarchical porous structure for bone regeneration, *Bio-Design and Manufacturing*, 3, 15–29, 2020.

[26] **H. Shao, J. He, T. Lin, Z. Zhang, Y. Zhang, and S. Liu**, 3D gel-printing of hydroxyapatite scaffold for bone tissue engineering, *Ceramics International*, 45, 1163–1170, 2019.

[27] **T. Zhou, L. Zhang, Q. Yao, Y. Ma, C. Hou, B. Sun, C. Shao, P. Gao, and H. Chen**, SLA 3D printing of high quality spine shaped β-TCP bioceramics for the hard tissue repair applications, *Ceramics International*, 46(6), 7609–7614, 2020.

[28] **J. Jeong, J. Kim, J. Shim, N. Hwang, and C. Heo**, Bioactive calcium phosphate materials and applications in bone regeneration, *Biomaterials Research*, 23, 4, 2019.

[29] **S. Pramanik, A. Agarwal, and K. Rai**, Development of high strength hydroxyapatite for hard tissue replacement, *Trends in Biomaterials and Artificial Organs,* 19, 46–51, 2005.

[30] **H. Chang and Y. Wang**, Cell responses to surface and architecture of tissue engineering scaffolds, in D. Eberli (ed.), *Regenerative medicine and tissue engineering — Cells and biomaterials*, London: Intech Open, 569-588, 2011.

[31] **T. Li, Y. Zhang, H. Ren, H. Peng, C. Lou, and J. Lin**, Two-step strategy for constructing hierarchical pore structured chitosan–hydroxyapatite composite scaffolds for bone tissue engineering, *Carbohydrate Polymers,* 260, 117765, 2021.

[32] **T. Putri, Sunarso, K. Hayashi, K. Tsuru, and K. Ishikawa**, Feasibility study on surface morphology regulation of β-tricalcium phosphate bone graft for enhancing cellular response, *Ceramics International*, 48(9), 13395–13399, 2022.

[33] **T. Hoepfner and E. Case**, The influence of microstructure on the hardness of sintered hydroxyapatite, *Ceramics International*, 29, 699–706, 2003.

[34] **E. Maevskaia, J. Guerrero, C. Ghayor, I. Bhattacharya, and F. Weber**, Triply periodic minimal surface-based scaffolds for bone tissue engineering: A mechanical, *in vitro* and *in vivo* study, *Tissue Engineering Part A*, 29(19-20), 507–517, 2023.